Large-range tuning and stabilization of the optical transition of diamond tin-vacancy centers by in situ strain control

Brevoord, Julia M.; Wienhoven, Leonardo G.C.; Codreanu, Nina; van Leeuwen, Elvis; Iuliano, Mariagrazia; De Santis, Lorenzo; Waas, Christopher; Beukers, Hans K.C.; Turan, Tim; Errando-Herranz, Carlos

DOI
10.1063/5.0251211

Publication date
2025

Document Version
Final published version

Published in
Applied Physics Letters

Applied Physics Letters

RESEARCH ARTICLE | APRIL 28 2025

Large-range tuning and stabilization of the optical transition of diamond tin-vacancy centers by *in situ* strain control

Special Collection: Quantum Networks

Julia M. Brevoord ; Leonardo G. C. Wienhoven ; Nina Codreanu ; Tetsuro Ishiguro ; Elvis van Leeuwen ; Mariagrazia Iuliano ; Lorenzo De Santis ; Christopher Waas ; Hans K. C. Beukers ; Tim Turan ; Carlos Errando-Herranz ; Kenichi Kawaguchi ; Ronald Hanson

Appl. Phys. Lett. 126, 174001 (2025)
https://doi.org/10.1063/5.0251211

AIP Publishing

Applied Physics Letters ARTICLE pubs.aip.org/aip/apl

Large-range tuning and stabilization of the optical transition of diamond tin-vacancy centers by *in situ* strain control

Cite as: Appl. Phys. Lett. **126**, 174001 (2025); doi: 10.1063/5.0251211
Submitted: 30 November 2024 · Accepted: 11 April 2025 ·
Published Online: 28 April 2025

Julia M. Brevoord,[1] Leonardo G. C. Wienhoven,[1] Nina Codreanu,[1] Tetsuro Ishiguro,[1,2] Elvis van Leeuwen,[1] Mariagrazia Iuliano,[1] Lorenzo De Santis,[1] Christopher Waas,[1] Hans K. C. Beukers,[1] Tim Turan,[1] Carlos Errando-Herranz,[1,3] Kenichi Kawaguchi,[2] and Ronald Hanson[1,a)]

AFFILIATIONS

[1]QuTech and Kavli Institute of Nanoscience, Delft University of Technology, Delft 2628 CJ, The Netherlands
[2]Quantum Laboratory, Fujitsu Limited, 10-1 Morinosato-Wakamiya, Atsugi, Kanagawa 243-0197, Japan
[3]Department of Quantum and Computer Engineering, Delft University of Technology, Delft 2628 CJ, The Netherlands

Note: This paper is part of the APL Special Topic, Quantum Networks.
[a)]**Author to whom correspondence should be addressed:** R.Hanson@tudelft.nl

ABSTRACT

The negatively charged tin-vacancy (SnV^-) center in diamond has emerged as a promising platform for quantum computing and quantum networks. To connect SnV^- qubits in large networks, *in situ* tuning and stabilization of their optical transitions are essential to overcome static and dynamic frequency offsets induced by the local environment. Here, we report on the large-range optical frequency tuning of diamond SnV^- centers using micro-electro-mechanically mediated strain control in photonic integrated waveguide devices. We realize a tuning range of >40 GHz, covering a major part of the inhomogeneous distribution. In addition, we employ real-time feedback on the strain environment to stabilize the resonance frequency and mitigate spectral wandering. These results provide a path for on-chip scaling of diamond SnV-based quantum networks.

Spin qubits in the solid state are promising building blocks for the realization of large-scale quantum systems,[1–8] with potential applications in computing and communication.[1,2] An early workhorse for the field has been the nitrogen-vacancy (NV) in diamond, which was used for a loophole-free Bell test,[9] the realization of a multi-node quantum network,[5] and heralded entanglement over metropolitan distances.[6] However, the relatively low Debye–Waller factor and the incompatibility with nanophotonic integration due to a first-order sensitivity to electrical noise limits the development of large-scale quantum networks and the integration into scalable photonic circuits based on NV centers in diamond. Next-generation color centers in solid state materials have started to emerge over the last decade to drive scaling of quantum systems.[8,10–13] The negatively charged tin-vacancy (SnV^-) center in diamond has attracted much recent attention due to its excellent optical properties,[14–16] high quantum efficiency,[17,18] and significant spin–orbit coupling,[19,20] which allows for operation above dilution refrigerator temperatures.[19,21,22] Furthermore, the SnV^- center lacks a first-order sensitivity to electrical noise due to its inversion symmetry, making it compatible with nanophotonic integration.[7,23–27] The recent demonstration of entanglement between the electron spin-1/2 SnV^- center and a nearby ^{13}C nuclear spin opens a path toward multi-qubit experiments using this platform.[22]

For connecting SnV^- qubits into larger networks, photonic links mediating entanglement generation provide a modular and scalable path.[28–31] The entanglement generation requires the qubits to emit indistinguishable photons. However, the photon emission of spin qubits in solids is typically not indistinguishable due to different local strain in the material resulting in a broad inhomogeneous distribution. In addition, the optical resonance frequency variations over time due to changes in, e.g., local strain and variations in the local electronic environment limit the indistinguishability of the emitted photons. This poses challenges for the realization of large-scale quantum networks. SnV^- centers in diamond are first-order insensitive to electric fields; therefore, conventional tuning using DC Stark tuning is limited.[32,33]

Previous work on strain engineering of other group-IV defects in diamond demonstrated frequency tuning,[10,34,35] the mitigation of phonon interactions,[36] and quantum interference of electromechanical stabilized emitters.[37] Recent work on strain engineering of SnV^- centers show heterogeneous integration with efficient state preparation and readout[7,25] and a tuning range up to ≈ 25 GHz. Here, we integrated diamond waveguide devices containing SnV^- centers with local optical frequency control via an electromechanically induced strain. We demonstrate a tuning range of >40 GHz and use the strain control in a feedback loop realizing a 12-fold improvement in the stabilization of the optical transition.

The SnV^- center in diamond consists of a tin-atom at the interstitial position between two missing carbon atoms with a captured electron, as shown in Fig. 1(a). A simplified level structure of the SnV^- center is given in Fig. 1(b). In the absence of a magnetic field, the ground and optically excited states are composed of spin-degenerate orbital doublets, resulting in four optical transitions.[17,38] In the presence of strain, the energy levels shift. In this work, we control the optical transition linking the lowest branch of the ground and the optically excited state, zero-phonon line (ZPL), the C-transition. The C-transition is well suited for spin readout and photon emission for photon-mediated entanglement generation. We study SnV^- centers in our device in an optical confocal set-up at an operating temperature of 4 K, see the supplementary material for more details on the experimental setup. The variation in optical resonances between different color centers in the diamond sample (inhomogeneous distribution) will determine the tuning range required to produce indistinguishable

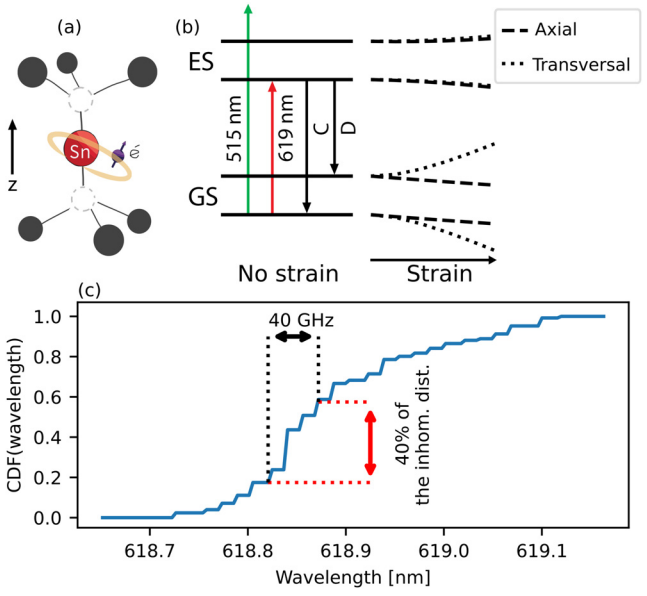

FIG. 1. (a) Schematic of the SnV^- center structure. (b) The energy level scheme of an SnV^- center in diamond, indicating the ground state (GS) splitting and the excited state (ES) splitting. We focus on tuning and stabilizing the C-transition, which is the most relevant for quantum technology applications. Resonant excitation at 619 nm results in zero-phonon line (ZPL) emission via the C-transition and the D-transition, as well as their respective phonon sidebands (PSB, not shown). Strain alters the energy levels. (c) The cumulative distribution function (CDF) of the inhomogeneous distribution from resonances obtained with PL.

photons from multiple color centers within the same diamond sample. The inhomogeneous distribution of the SnV^- centers in the devices fabricated on a diamond sample used for this work is determined by photoluminescence (PL) measurements. We collect the emission in free space using a spectrometer while illuminating the sample with an off-resonant 515 nm laser with 200 μW and integrating over 10 s at 173 different laser spot locations on different devices. We determine the resonances of the C-transition using a peak-finding algorithm. The cumulative inhomogeneous distribution is plotted in Fig. 1(c). About 40% of the resonances detected in the region of interest are within a 40 GHz window. This range is not a fundamental limitation, in the recent work of Li *et al.*,[7] they found 40% of the resonances in a ≈ 20 GHz window. Moreover, Görlitz *et al.* reported a linewidth of 15 GHz for the ZPL transition of an ensemble of SnV centers in a high-pressure, high-temperature annealed diamond implanted with Sn atoms.[18] In addition to overcoming this static inhomogeneity, spectral diffusion and bi-stability pose a second challenge, as reported by others.[15,24,26,39–41] In this work, we target both challenges using *in situ* strain engineering of the SnV^-, including real-time feedback.

Following Meesala *et al.*[35] and Guo *et al.*,[21] considering an infinitesimal strain regime, we use the Hamiltonian describing strain in the basis of the SnV^-,

$$\mathbb{H}_{\text{strain}} = \sum_{i,j} A_{ij}\epsilon_{ij}, \tag{1}$$

where ϵ_{ij} is a component of the strain tensor, $\boldsymbol{\epsilon}$, and A_{ij} operators that act on the electronic levels. Using group theory, we can write the Hamiltonian in the irreducible representations of the D_{3d} point group, on the basis $\{|e_x\uparrow\rangle, |e_x\downarrow\rangle, |e_y\uparrow\rangle, |e_y\downarrow\rangle\}$, where e_x, e_y represent the orbital and $\downarrow$, $\uparrow$ the electronic spin-1/2 states. This shows that strain does not couple the ground and excited states, resulting in identical strain Hamiltonians forms for the ground and excited states. In this basis and in the local coordinate frame of the SnV^- center, where z is along the high-symmetry axis, the [111] crystallographic direction, the part of the Hamiltonian describing the presence of strain is

$$\mathbb{H}_{\text{strain}} = \begin{bmatrix} \epsilon_{A_{1g}} - \epsilon_{E_{gx}} & \epsilon_{E_{gy}} \\ \epsilon_{E_{gy}} & \epsilon_{A_{1g}} + \epsilon_{E_{gx}} \end{bmatrix} \otimes \mathbb{I}_2, \tag{2}$$

where $\epsilon_{A_{1g}}, \epsilon_{E_{gx}}, \epsilon_{E_{gy}}$ represent the strain induced deformation modes in the D_{3d} point group. Rewriting each term as a linear combination of the strain tensor results in

$$\begin{aligned} \epsilon_{A_{1g}} &= t_\perp(\epsilon_{xx} + \epsilon_{yy}) + t_\parallel \epsilon_{zz}, \\ \epsilon_{E_{gx}} &= d(\epsilon_{xx} - \epsilon_{yy}) + f\epsilon_{zx}, \\ \epsilon_{E_{gy}} &= -2d\epsilon_{xy} + f\epsilon_{yz}, \end{aligned} \tag{3}$$

where $t_\perp$, $t_\parallel$, d, and f are the strain susceptibilities, with different values in the ground and excited state. Diagonalizing the Hamiltonian and including spin–orbit coupling results in expressions for the mean ZPL frequency, ν_{ZPL}, and ground and excited state splitting, $\Delta_{u,g}$,

$$\begin{aligned} \nu_{\text{ZPL}} &= \nu_0 + \epsilon^u_{A_{1g}} - \epsilon^g_{A_{1g}}, \\ \Delta_u &= \sqrt{(\lambda^u_{SO})^2 + 4(\epsilon^u_{E_{gx}})^2 + 4(\epsilon^u_{E_{gy}})^2}, \\ \Delta_g &= \sqrt{(\lambda^g_{SO})^2 + 4(\epsilon^g_{E_{gx}})^2 + 4(\epsilon^g_{E_{gy}})^2}, \end{aligned} \tag{4}$$

where ν_0 is the mean ZPL frequency in the absence of strain and $\lambda_{SO}^{g,(u)}$ is the spin–orbit coupling of the ground (excited) state. The superscript g (u) indicates the ground (excited) state contribution.

Our investigation focuses on SnV^- centers embedded in waveguide-based microelectromechanical system (MEMS) devices. Figure 2(a) shows a false-colored scanning electron microscope (SEM) image of the full MEMS device. The SnV^- incorporated waveguide is on one side connected via a mechanical spring-like structure to the bulk, and on the other side clamped by two bars to two diamond bulk support platforms. Niobium electrodes (with titanium as the adhesion layer) are deposited on the spring (top electrode), indicated by the blue-colored region in Fig. 2(a), and below the spring (bottom electrode), indicated by the purple shaded region on Fig. 2(a). These electrodes form a capacitive electromechanical actuator when a bias voltage is applied between the electrodes. According to Eq. (4), by varying the applied bias voltage, we can tune the optical resonance frequency of the SnV^- center due to the induced strain in the crystal.

Our device is fabricated from an electronic grade ⟨001⟩ -surface-orientated diamond sample. The Sn atoms are uniformly implanted with a dose of 10^{11} ions/cm^2. After vacuum-annealing to activate the SnV^- centers, the color centers are predicted to end up at a mean depth of 90 nm below the surface with a straggle of 17 nm from stopping and range of ions in matter (SRIM) simulations.[42] Due to substantial graphite formation during vacuum-annealing, an additional short plasma etching step was performed to remove the graphitic layer, resulting in SnV^- centers closer to the surface. Fabrication details can be found in the supplementary material. The waveguides used in this work are longitudinally aligned along the [110] direction. The four possible orientations of the SnV^-centers in the diamond crystal are [111], [$\bar{1}$ 11], [1 $\bar{1}$ 1], and [$\bar{1}\bar{1}$ 1]. Considering the dominant uniaxial strain along the [110] direction when a voltage is applied, two groups of color centers that respond similarly to strain remain, indicated in Fig. 2(b). We denote the SnV^- centers with a component of the dipole along (perpendicular) the long axis of the beam as axial (transversal) color centers.

We perform a finite element method (FEM) simulation using Ansys[43] to determine the strain in the waveguide when a voltage is applied over the electrodes. The ϵ_{xx} (lab frame) component of the strain tensor on the surface of the beam is shown in Fig. 2(c) when 75 V is applied, resulting in a maximal strain of $\epsilon_{xx} = 7 \times 10^{-5}$. Additional information on the simulations can be found in the supplementary material. We have indicated the estimated position

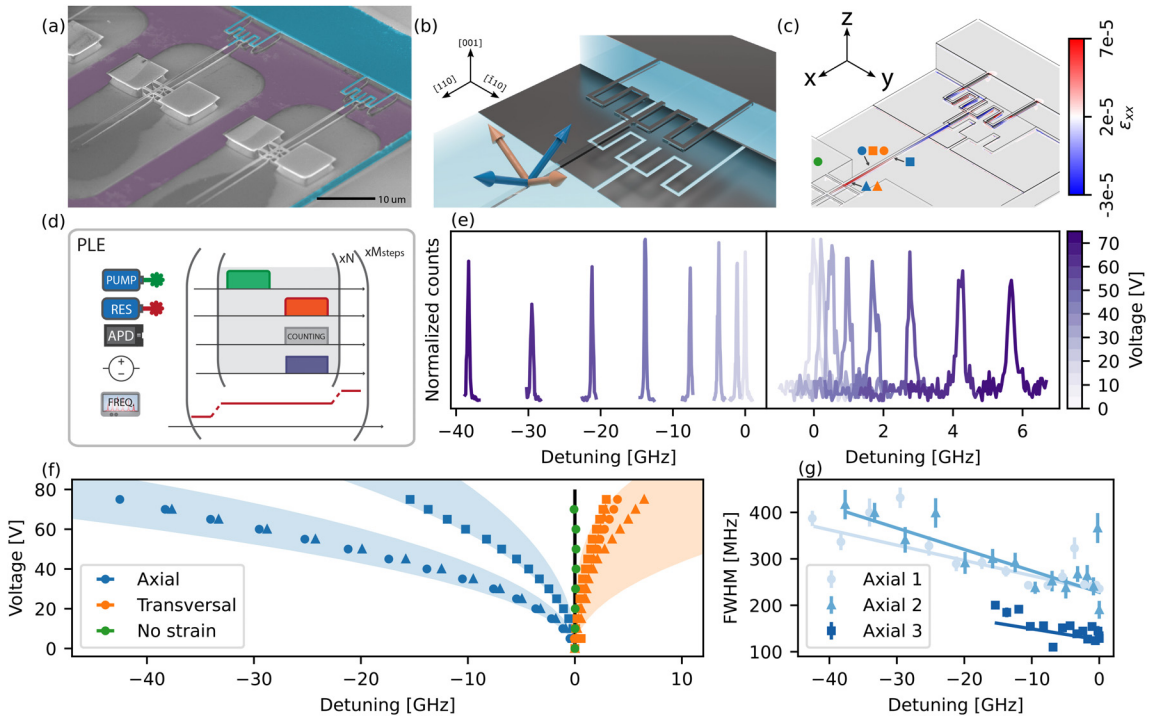

FIG. 2. (a) False colored scanning electron microscope (SEM) image of the devices. (b) Orientation of the axial (transversal) SnV^- centers in the waveguide, indicated by the blue (orange) arrows. (c) Finite element method (FEM) simulation of the strain distribution (ϵ_{xx} component) over the surface of the device when 75 V is applied. The estimated positions of the SnV^- centers evaluated in (f) are indicated. (d) Pulse sequence of a photoluminescence excitation (PLE) scan, consisting of a pump off-resonant green pulse, a resonant (res) laser pulse, and photon counting by an avalanche photodiode (APD). (e) Fluorescence of PLE scans taken at different bias voltages of an axial (blue triangle) [transversal (orange triangle)] SnV^- center in the left (right) panel, showing an optical frequency shift of almost −40 GHz (6 GHz). The fluorescence is normalized to the maximal count rate of the 0 V scan for the axial (8680 counts/s) and transversal emitter (2320 counts/s). (f) Summary of the measured optical resonance frequency detuning of several SnV^- centers, indicated by different shaped data points, as a function of the applied bias voltage, the error bars lie within the data points. The shaded areas are the simulated frequency shift as a function of the applied bias voltage for the SnV^- center 20 nm below the surface at the hinge point (orange and blue triangle) and 4 μm away from it (blue square), the uncertainty is in the depth of the color center and the strain susceptibility parameter $t_\perp$. (g) A summary of the obtained full-width half maximum (FWHM) from fitting PLE scan fluorescence as a function of detuning, for multiple axial oriented SnV^- centers, which we have fitted with a linear function.

of the SnV^- centers, positioned in different waveguides, evaluated in this work.

By rotating the strain tensor obtained from the FEM simulation from the lab frame to the axial/transversal SnV^- center reference frame and using Eqs. (3) and (4), we simulate the resonance frequency shift of SnV^- centers in our device as a function of applied voltage. We use the strain susceptibilities d and f determined by Guo and Stramma *et al.*[21] and $t_{\parallel}$ from studies on other group-IV color centers by Meesala and Sohn *et al.*,[35] and Maity and Shao *et al.*[34] We note that using the single reported value for $t_{\parallel}$ for SnV^- in Ref. 25 resulted in a discrepancy with the data well outside the uncertainty margin. For $t_{\perp}$, we take a lower and an upper bound based on reported values for other group-IV color centers,[34,35] and incorporate this into the uncertainty margins of our simulations.

To determine the tuning range of the SnV^- centers in this sample, we perform photoluminescence excitation (PLE) scans using the pulse sequence shown in Fig. 2(d). We record the phonon sideband (PSB) emission during the PLE scans. The bias voltage is applied in a pulsed way concurrent with the resonant readout to avoid heating originating from leakage current in the system. We have calibrated the pulse time and the time between subsequent pulses to eliminate the effects of heating. More information on the calibration can be found in the supplementary material.

Figure 2(e) shows the PSB collection during PLE scans for different applied bias voltages. We observe the two distinct tuning behaviors attributed to the axial and transversal-oriented groups. The results of multiple SnV^- centers are summarized in Fig. 2(f), where we plot the detuning as a function of the applied bias voltage. In the supplementary material, we plot the absolute frequency shift as a function of the applied voltage. From the emitters evaluated, we can tune 4 pairs of emitters to the same absolute frequency. For an axial and a transversal SnV^- center positioned close to the hinge point [indicated by the orange and blue triangles in Fig. 2(c)] and an axial SnV^- center further away from the hinge point (indicated by the blue square), we simulate the expected frequency shift, indicated by the shaded areas in Fig. 2(f). We included an error bar representing our uncertainty in the depth of the color centers in the beam and the strain susceptibility values. The optical resonance of an SnV^- in the bulk (indicated by the green circle), which should not experience strain due to the bias voltage, is recorded for reference. This reference SnV^- indeed shows no frequency shift with increasing voltage. We find that SnV^- centers that show axial SnV^- center behavior can be tuned up to ≈ 43 GHz and transversal centers up to ≈ 6 GHz, covering a substantial part of the inhomogeneous distribution.

We observe a linear increase in the linewidth with frequency shift and hence strain in Fig. 2(g), where we summarize the fitted full-width half maximum (FWHM) of the linewidth obtained from the PLE scans of several axial SnV^- centers. We observe a similar trend for these color centers, with a mean linewidth increase in 3.42 MHz/GHz. We did not see this behavior for the reference emitter evaluated in the bulk. Further investigation is needed to determine whether this behavior is intrinsic to SnV^- centers or device-related (e.g., induced by local heating).

The second challenge that we address in this work is the optical transition frequency drift over time. Drifts of the optical resonance frequency due to changes in the local charge environment can be compensated by real-time logic protocols, called charge resonance (CR) checks, that can herald the desired resonance condition.[15,44] This method relies on applying an off-resonant pulse, which alters the local charge environment. However, drifts beyond the local charge-induced distribution will lead to vanishing heralding success probabilities for these protocols. In those cases, the drift can be compensated for by dynamically adjusting the local strain.[45] We implement a real-time feedback loop, utilizing strain tuning to stabilize the SnV^- center at a desired resonant optical frequency. The experimental protocol is schematically depicted in Fig. 3(a). It starts with a resonant readout pulse at the target resonance frequency while counting the PSB photons. We superimpose the strain-inducing DC bias voltage with a sinusoidal signal and correlate the number of counts with the phase of the control modulation signal. This is followed by a CR check. Once this is passed, the experimental sequence is started. By averaging the photon counts obtained during the gate modulation phase of this sequence, we obtain an error signal to adjust the static DC bias voltage using a standard

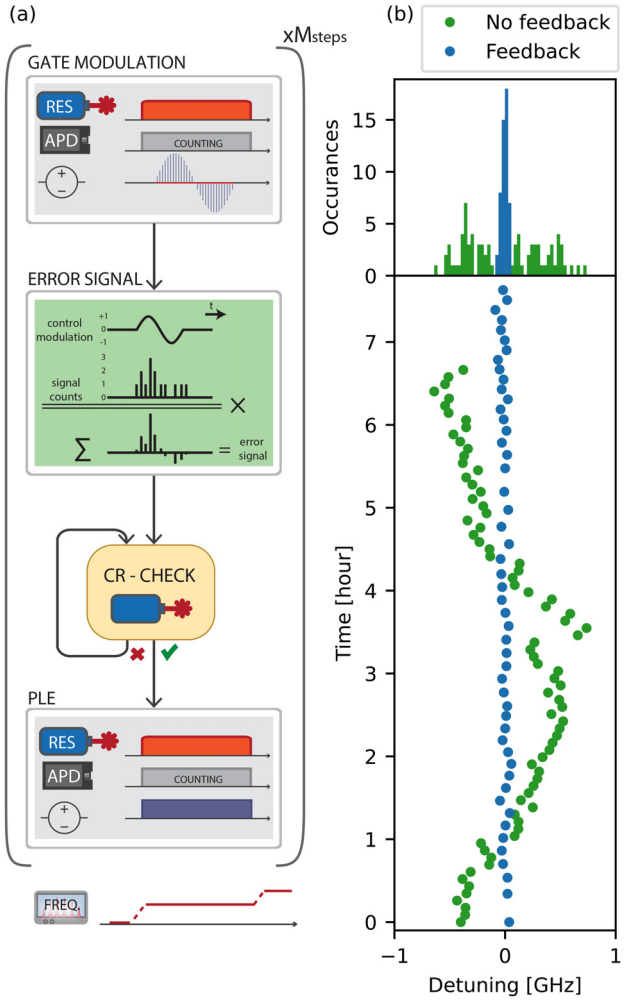

FIG. 3. (a) Pulse sequence and real-time logic of the gate-modulated CR-checked PLE. (b) (Bottom panel) Fitted centers of the fluorescence of 50 gate-modulated CR-checked PLE scans, taken over 7 h. For comparison the fitted centers of PLE scans with no active feedback in green. The error bar lies within the data points. (Top panel) Histogram of the fitted centers.

proportional–integral–derivative (PID) feedback loop. The strain-inducing DC bias voltage is updated at a 5 Hz rate. This method effectively compensates for slow drifts limited by the update rate and can be used complementarily to the CR check, which addresses faster and smaller drifts in the optical resonance frequency.

To test the stability, we probe the resonance frequency of an SnV^- for more than 7 h by PLE scans. We fit the photon counts recorded per scan with a Voigt function and plot the fitted center frequency as a function of time in Fig. 3(b) bottom panel. The stability observed over the 7-h duration demonstrates the robustness of the system, and there are no intrinsic limitations that would preclude maintaining this stability over extended time periods. When no active feedback is applied, the drifts of the optical resonance are larger than can be compensated for by changes in the local charge environment. We compare the gate-modulated CR-checked PLE scans with PLE scans when no active feedback or CR checks are applied. The standard deviation of the fitted centers with active feedback is 30 MHz, while for the non-feedback case, the standard deviation is 365 MHz. In the top panel of Fig. 3(b), we plot a histogram of the fitted centers. The FWHM of the summed counts is 229 ± 2 MHz and the mean of the FWHM of the individual fitted scans is 225 MHz. Comparing the standard deviation in fitted centers with the non-feedback case results in a 12-fold increase in optical frequency stability with this feedback technique.

In summary, we have presented and demonstrated fabricated devices that show a tunability up to >40 GHz, covering a significant part of the inhomogeneous distribution of the SnV^- centers in this sample. We have stabilized the optical resonance of an SnV^- using a dynamic strain feedback loop and demonstrated a 12-fold improvement in stability. The strain tuning is applied locally to SnV^- embedded in waveguides and can be extended to tune numerous SnV^- on the same chip simultaneously. The methods demonstrated here pave the way toward the generation of heralded indistinguishable photons from many integrated SnV^- qubits, providing an important element for scaling SnV^--based quantum technologies.

See the supplementary material for a description of the fabrication of the device used in this work, the experimental setup with which the measurements were performed, a description of the voltage pulse calibration, a plot of the absolute frequency shift as a function of the applied voltage, and further details about the FEM simulations.

The authors thank R. Schouten and B. Otto for electronic support, N. Albers for machining parts of the experimental setup, and O. Benningshof and J. Mensingh for cryogenics matter. The authors thank V. V. Dobrovitski for the fruitful discussions and A. Stramma for proofreading the manuscript. We acknowledge support from the joint research program "Modular quantum computers" by Fujitsu Limited and Delft University of Technology, co-funded by the Netherlands Enterprise Agency under Project No. PPS2007, from the Dutch Research Council (NWO) through the Spinoza prize 2019 (Project No. SPI 63-264), from the Dutch Ministry of Economic Affairs and Climate Policy (EZK) as part of the Quantum Delta NL program, from the Quantum Internet Alliance through the Horizon Europe program (Grant Agreement No. 101080128), and from the European Union's Horizon Europe research and innovation program under Grant Agreement No. 101102140—QIA Phase 1.

AUTHOR DECLARATIONS

Conflict of Interest

The authors have no conflicts to disclose.

Author Contributions

Julia M. Brevoord: Conceptualization (lead); Data curation (lead); Formal analysis (lead); Investigation (lead); Methodology (lead); Software (lead); Validation (lead); Visualization (lead); Writing – review & editing (lead). **Leonardo G. C. Wienhoven:** Conceptualization (lead); Formal analysis (equal); Investigation (lead); Methodology (equal); Software (equal); Validation (equal); Visualization (lead); Writing – review & editing (equal). **Nina Codreanu:** Conceptualization (equal); Investigation (supporting); Methodology (equal); Writing – review & editing (supporting). **Tetsuro Ishiguro:** Conceptualization (equal); Investigation (equal); Methodology (equal); Writing – review & editing (supporting). **Elvis van Leeuwen:** Conceptualization (equal); Investigation (supporting); Methodology (equal); Writing – review & editing (supporting). **Mariagrazia Iuliano:** Methodology (equal); Software (supporting); Writing – review & editing (supporting). **Lorenzo De Santis:** Conceptualization (equal); Methodology (equal); Writing – review & editing (supporting). **Christopher Waas:** Investigation (equal); Methodology (equal); Software (supporting); Writing – review & editing (supporting). **Hans K. C. Beukers:** Methodology (equal); Software (supporting); Writing – review & editing (supporting). **Tim Turan:** Methodology (equal); Software (supporting); Writing – review & editing (supporting). **Carlos Errando-Herranz:** Methodology (equal); Writing – review & editing (supporting). **Kenichi Kawaguchi:** Methodology (equal); Supervision (equal); Writing – review & editing (supporting). **Ronald Hanson:** Conceptualization (lead); Funding acquisition (lead); Project administration (lead); Resources (lead); Supervision (lead); Validation (equal); Writing – review & editing (equal).

DATA AVAILABILITY

The data that support the findings of this study are openly available in 4TU.ResearchData at https://www.doi.org/10.4121/6b89815e-d73c-4abd-93cc-a0514c2780ae, Ref. 46.

REFERENCES

[1]H. J. Kimble, "The quantum internet," Nature **453**, 1023–1030 (2008).
[2]S. Wehner, D. Elkouss, and R. Hanson, "Quantum internet: A vision for the road ahead," Science **362**, eaam9288 (2018).
[3]P.-J. Stas, Y. Q. Huan, B. Machielse, E. N. Knall, A. Suleymanzade, B. Pingault, M. Sutula, S. W. Ding, C. M. Knaut, D. R. Assumpcao, Y.-C. Wei, M. K. Bhaskar, R. Riedinger, D. D. Sukachev, H. Park, M. Lončar, D. S. Levonian, and M. D. Lukin, "Robust multi-qubit quantum network node with integrated error detection," Science **378**, 557–560 (2022).
[4]C. T. Nguyen, D. D. Sukachev, M. K. Bhaskar, B. Machielse, D. S. Levonian, E. N. Knall, P. Stroganov, C. Chia, M. J. Burek, R. Riedinger, H. Park, M. Lončar, and M. D. Lukin, "An integrated nanophotonic quantum register based on silicon-vacancy spins in diamond," Phys. Rev. B **100**, 165428 (2019).
[5]M. Pompili, S. L. N. Hermans, S. Baier, H. K. C. Beukers, P. C. Humphreys, R. N. Schouten, R. F. L. Vermeulen, M. J. Tiggelman, L. D. S. Martins, B. Dirkse,

S. Wehner, and R. Hanson, "Realization of a multinode quantum network of remote solid-state qubits," Science **372**, 259–264 (2021).
[6]A. J. Stolk, K. L. van der Enden, M.-C. Slater, I. T. Raa-Derckx, P. Botma, J. van Rantwijk, J. J. B. Biemond, R. A. J. Hagen, R. W. Herfst, W. D. Koek, A. J. H. Meskers, R. Vollmer, E. J. van Zwet, M. Markham, A. M. Edmonds, J. F. Geus, F. Elsen, B. Jungbluth, C. Haefner, C. Tresp, J. Stuhler, S. Ritter, and R. Hanson, "Metropolitan-scale heralded entanglement of solid-state qubits," Sci. Adv. **10**, eadp6442 (2024).
[7]L. Li, L. D. Santis, I. B. W. Harris, K. C. Chen, Y. Gao, I. Christen, H. Choi, M. Trusheim, Y. Song, C. Errando-Herranz, J. Du, Y. Hu, G. Clark, M. I. Ibrahim, G. Gilbert, R. Han, and D. Englund, "Heterogeneous integration of spin–photon interfaces with a CMOS platform," Nature **630**, 70–76 (2024).
[8]M. K. Bhaskar, R. Riedinger, B. Machielse, D. S. Levonian, C. T. Nguyen, E. N. Knall, H. Park, D. Englund, M. Lončar, D. D. Sukachev, and M. D. Lukin, "Experimental demonstration of memory-enhanced quantum communication," Nature **580**, 60–64 (2020).
[9]B. Hensen, H. Bernien, A. E. Dréau, A. Reiserer, N. Kalb, M. S. Blok, J. Ruitenberg, R. F. L. Vermeulen, R. N. Schouten, C. Abellán, W. Amaya, V. Pruneri, M. W. Mitchell, M. Markham, D. J. Twitchen, D. Elkouss, S. Wehner, T. H. Taminiau, and R. Hanson, "Loophole-free Bell inequality violation using electron spins separated by 1.3 kilometres," Nature **526**, 682–686 (2015).
[10]N. H. Wan, T.-J. Lu, K. C. Chen, M. P. Walsh, M. E. Trusheim, L. De Santis, E. A. Bersin, I. B. Harris, S. L. Mouradian, I. R. Christen, E. S. Bielejec, and D. Englund, "Large-scale integration of artificial atoms in hybrid photonic circuits," Nature **583**, 226–231 (2020).
[11]J. Heiler, J. Körber, E. Hesselmeier, P. Kuna, R. Stöhr, P. Fuchs, M. Ghezellou, J. Ul-Hassan, W. Knolle, C. Becher, F. Kaiser, and J. Wrachtrup, "Spectral stability of V2 centres in sub-micron 4H-SiC membranes," npj Quantum Mater. **9**, 34 (2024).
[12]S. Simmons, "Scalable fault-tolerant quantum technologies with silicon color centers," PRX Quantum **5**, 010102 (2024).
[13]M. Bhaskar, D. Sukachev, A. Sipahigil, R. Evans, M. Burek, C. Nguyen, L. Rogers, P. Siyushev, M. Metsch, H. Park, F. Jelezko, M. Lončar, and M. Lukin, "Quantum nonlinear optics with a germanium-vacancy color center in a nanoscale diamond waveguide," Phys. Rev. Lett. **118**, 223603 (2017).
[14]M. E. Trusheim, B. Pingault, N. H. Wan, M. Gündoğan, L. De Santis, R. Debroux, D. Gangloff, C. Purser, K. C. Chen, M. Walsh, J. J. Rose, J. N. Becker, B. Lienhard, E. Bersin, I. Paradeisanos, G. Wang, D. Lyzwa, A. R.-P. Montblanch, G. Malladi, H. Bakhru, A. C. Ferrari, I. A. Walmsley, M. Atatüre, and D. Englund, "Transform-limited photons from a coherent tin-vacancy spin in diamond," Phys. Rev. Lett. **124**, 023602 (2020).
[15]J. M. Brevoord, L. De Santis, T. Yamamoto, M. Pasini, N. Codreanu, T. Turan, H. K. Beukers, C. Waas, and R. Hanson, "Heralded initialization of charge state and optical-transition frequency of diamond tin-vacancy centers," Phys. Rev. Appl. **21**, 054047 (2024).
[16]A. E. Rugar, S. Aghaeimeibodi, D. Riedel, C. Dory, H. Lu, P. J. McQuade, Z.-X. Shen, N. A. Melosh, and J. Vučković, "Quantum photonic interface for tin-vacancy centers in diamond," Phys. Rev. X **11**, 031021 (2021).
[17]T. Iwasaki, Y. Miyamoto, T. Taniguchi, P. Siyushev, M. H. Metsch, F. Jelezko, and M. Hatano, "Tin-vacancy quantum emitters in diamond," Phys. Rev. Lett. **119**, 253601 (2017).
[18]J. Görlitz, D. Herrmann, G. Thiering, P. Fuchs, M. Gandil, T. Iwasaki, T. Taniguchi, M. Kieschnick, J. Meijer, M. Hatano, A. Gali, and C. Becher, "Spectroscopic investigations of negatively charged tin-vacancy centres in diamond," New J. Phys. **22**, 013048 (2020).
[19]E. I. Rosenthal, C. P. Anderson, H. C. Kleidermacher, A. J. Stein, H. Lee, J. Grzesik, G. Scuri, A. E. Rugar, D. Riedel, S. Aghaeimeibodi, G. H. Ahn, K. Van Gasse, and J. Vučković, "Microwave spin control of a tin-vacancy qubit in diamond," Phys. Rev. X **13**, 031022 (2023).
[20]I. Karapatzakis, J. Resch, M. Schrodin, P. Fuchs, M. Kieschnick, J. Heupel, L. Kussi, C. Sürgers, C. Popov, J. Meijer, C. Becher, W. Wernsdorfer, and D. Hunger, "Microwave control of the tin-vacancy spin qubit in diamond with a superconducting waveguide," Phys. Rev. X **14**, 031036 (2024).
[21]X. Guo, A. M. Stramma, Z. Li, W. G. Roth, B. Huang, Y. Jin, R. A. Parker, J. Arjona Martínez, N. Shofer, C. P. Michaels, C. P. Purser, M. H. Appel, E. M. Alexeev, T. Liu, A. C. Ferrari, D. D. Awschalom, N. Delegan, B. Pingault, G. Galli, F. J. Heremans, M. Atatüre, and A. A. High, "Microwave-based quantum control and coherence protection of tin-vacancy spin qubits in a strain-tuned diamond-membrane heterostructure," Phys. Rev. X **13**, 041037 (2023).
[22]H. K. C. Beukers, C. Waas, M. Pasini, H. B. van Ommen, Z. Ademi, M. Iuliano, N. Codreanu, J. M. Brevoord, T. Turan, T. H. Taminiau, and R. Hanson, "Control of solid-state nuclear spin qubits using an electron spin-1/2," arXiv:2409.08977 (2024).
[23]A. E. Rugar, C. Dory, S. Sun, and J. Vučković, "Characterization of optical and spin properties of single tin-vacancy centers in diamond nanopillars," Phys. Rev. B **99**, 205417 (2019).
[24]M. Pasini, N. Codreanu, T. Turan, A. Riera Moral, C. F. Primavera, L. De Santis, H. K. Beukers, J. M. Brevoord, C. Waas, J. Borregaard, and R. Hanson, "Nonlinear quantum photonics with a tin-vacancy center coupled to a one-dimensional diamond waveguide," Phys. Rev. Lett. **133**, 023603 (2024).
[25]G. Clark, H. Raniwala, M. Koppa, K. Chen, A. Leenheer, M. Zimmermann, M. Dong, L. Li, Y. H. Wen, D. Dominguez, M. Trusheim, G. Gilbert, M. Eichenfield, and D. Englund, "Nanoelectromechanical control of spin–photon interfaces in a hybrid quantum system on chip," Nano Lett. **24**, 1316 (2024).
[26]J. Arjona Martínez, R. A. Parker, K. C. Chen, C. M. Purser, L. Li, C. P. Michaels, A. M. Stramma, R. Debroux, I. B. Harris, M. Hayhurst Appel, E. C. Nichols, M. E. Trusheim, D. A. Gangloff, D. Englund, and M. Atatüre, "Photonic indistinguishability of the tin-vacancy center in nanostructured diamond," Phys. Rev. Lett. **129**, 173603 (2022).
[27]C. Bradac, W. Gao, J. Forneris, M. E. Trusheim, and I. Aharonovich, "Quantum nanophotonics with group IV defects in diamond," Nat. Commun. **10**, 5625 (2019).
[28]M. Ruf, N. H. Wan, H. Choi, D. Englund, and R. Hanson, "Quantum networks based on color centers in diamond," J. Appl. Phys. **130**, 070901 (2021).
[29]H. Choi, M. Pant, S. Guha, and D. Englund, "Percolation-based architecture for cluster state creation using photon-mediated entanglement between atomic memories," npj Quantum Inf. **5**, 1–7 (2019).
[30]N. H. Nickerson, J. F. Fitzsimons, and S. C. Benjamin, "Freely scalable quantum technologies using cells of 5-to-50 qubits with very lossy and noisy photonic links," Phys. Rev. X **4**, 041041 (2014).
[31]K. Nemoto, M. Trupke, S. J. Devitt, A. M. Stephens, B. Scharfenberger, K. Buczak, T. Nöbauer, M. S. Everitt, J. Schmiedmayer, and W. J. Munro, "Photonic architecture for scalable quantum information processing in diamond," Phys. Rev. X **4**, 031022 (2014).
[32]L. De Santis, M. Trusheim, K. Chen, and D. Englund, "Investigation of the Stark effect on a centrosymmetric quantum emitter in diamond," Phys. Rev. Lett. **127**, 147402 (2021).
[33]S. Aghaeimeibodi, D. Riedel, A. E. Rugar, C. Dory, and J. Vučković, "Electrical tuning of tin-vacancy centers in diamond," Phys. Rev. Appl. **15**, 064010 (2021).
[34]S. Maity, L. Shao, Y.-I. Sohn, S. Meesala, B. Machielse, E. Bielejec, M. Markham, and M. Lončar, "Spectral alignment of single-photon emitters in diamond using strain gradient," Phys. Rev. Appl. **10**, 024050 (2018).
[35]S. Meesala, Y.-I. Sohn, B. Pingault, L. Shao, H. A. Atikian, J. Holzgrafe, M. Gundogan, C. Stavrakas, A. Sipahigil, C. Chia, M. J. Burek, M. Zhang, L. Wu, J. L. Pacheco, J. Abraham, E. Bielejec, M. D. Lukin, M. Atature, and M. Loncar, "Strain engineering of the silicon-vacancy center in diamond," Phys. Rev. B **97**, 205444 (2018).
[36]Y.-I. Sohn, S. Meesala, B. Pingault, H. A. Atikian, J. Holzgrafe, M. Gündoğan, C. Stavrakas, M. J. Stanley, A. Sipahigil, J. Choi, M. Zhang, J. L. Pacheco, J. Abraham, E. Bielejec, M. D. Lukin, M. Atatüre, and M. Lončar, "Controlling the coherence of a diamond spin qubit through its strain environment," Nat. Commun. **9**, 2012 (2018).
[37]B. Machielse, S. Bogdanovic, S. Meesala, S. Gauthier, M. Burek, G. Joe, M. Chalupnik, Y. Sohn, J. Holzgrafe, R. Evans, C. Chia, H. Atikian, M. Bhaskar, D. Sukachev, L. Shao, S. Maity, M. Lukin, and M. Lončar, "Quantum interference of electromechanically stabilized emitters in nanophotonic devices," Phys. Rev. X **9**, 031022 (2019).
[38]C. Hepp, T. Müller, V. Waselowski, J. N. Becker, B. Pingault, H. Sternschulte, D. Steinmüller-Nethl, A. Gali, J. R. Maze, M. Atatüre, and C. Becher, "Electronic structure of the silicon vacancy color center in diamond," Phys. Rev. Lett. **112**, 036405 (2014).
[39]G. Pieplow, C. G. Torun, J. H. D. Munns, F. M. Herrmann, A. Thies, T. Pregnolato, and T. Schröder, "Quantum electrometer for time-resolved material science at the atomic lattice scale," arXiv:2401.14290 (2024).

[40]Y. Herrmann, J. Fischer, J. M. Brevoord, C. Sauerzapf, L. G. Wienhoven, L. J. Feije, M. Pasini, M. Eschen, M. Ruf, M. J. Weaver, and R. Hanson, "Coherent coupling of a diamond tin-vacancy center to a tunable open microcavity," Phys. Rev. X **14**, 041013 (2024).
[41]Z. Li, X. Guo, Y. Jin, F. Andreoli, A. Bilgin, D. D. Awschalom, N. Delegan, F. J. Heremans, D. Chang, G. Galli, and A. A. High, "Atomic optical antennas in solids," Nat. Photonics **18**, 1113 (2024).
[42]J. F. Ziegler, M. Ziegler, and J. Biersack, "SRIM—The stopping and range of ions in matter (2010)," Nucl. Instrum. Methods Phys. Res., Sect. B **268**, 1818–1823 (2010).
[43]"Ansys® Academic Research Mechanical, Release 18.1."
[44]H. Bernien, B. Hensen, W. Pfaff, G. Koolstra, M. S. Blok, L. Robledo, T. H. Taminiau, M. Markham, D. J. Twitchen, L. Childress, and R. Hanson, "Heralded entanglement between solid-state qubits separated by three metres," Nature **497**, 86–90 (2013).
[45]V. M. Acosta, C. Santori, A. Faraon, Z. Huang, K.-M. C. Fu, A. Stacey, D. A. Simpson, K. Ganesan, S. Tomljenovic-Hanic, A. D. Greentree, S. Prawer, and R. G. Beausoleil, "Dynamic stabilization of the optical resonances of single nitrogen-vacancy centers in diamond," Phys. Rev. Lett. **108**, 206401 (2012).
[46]J. M. Brevoord, L. Wienhoven, N. Codreanu, T. Ishiguro, E. van Leeuwen, M. Iuliano, L. De Santis, C. Waas, H. K. C. Beukers, T. L. Turan, C. Errando-Herranz, K. Kawaguchi, and R. Hanson (2024). "Data underlying the publication 'Large-range tuning and stabilization of the optical transition of diamond tin-vacancy centers by in-situ strain control,'" 4TU.ResearchData. https://www.doi.org/10.4121/6b89815e-d73c-4abd-93cc-a0514c2780ae